Influence of Frictional or Rotational Kinetic Energy on Wellbore-Fluid/Temperature Profiles During Drilling Operations

A. Q. Al Saedi and **R. E. Flori,** Missouri University of Science and Technology, and
C. S. Kabir, Missouri University of Science and Technology and University of Houston

Summary

Temperature-profile distributions in a wellbore during drilling operations might take different forms when applying the energy balance in the overall system. For steady-state conditions, wherein the wellbore is considered a closed system, adding any source of additional energy to this system can influence the predicted temperature profiles. This study presents a new analytical model to investigate the influence of rotational energy arising from the drillstring operation on the wellbore-temperature behavior.

A significant part of the drilling operation is rotation of the drillstring. Depending on the drilling rig, various equipment provides this kind of energy, such as the rotary table or topdrive. In addition, downhole motors or turbines can add additional rotation to the drill bit. This type of energy source can be construed as a supplemental heat source that could be added to the formulations of drillpipe- and annular-temperature profiles.

Overall, this study presents two models involving frictional and rotational energy. These models yield the same solution if we do not include the energy source, and they can apply equally well for any energy-balance system. The proposed mathematical models provide new insights into different energy terms that can be included to compute the temperature profiles in the drillpipe and annulus.

Introduction

The importance of temperature profiles for both tubular and annular conduits in wellbores underlies the influence of those temperatures on further operations and fluid properties. Moreover, an additional heat source might also influence the tools' longevity.

In drilling operations, the frictional forces originate from pressure losses or the contact area between the drilling tool and the drilled formation. Furthermore, the torque-and-drag forces result from rotating the drillstring, as reported by Samuel (2007), Aadnoy and Djurhuus (2008), Aadnoy et al. (2010), and Mirhaj et al. (2016). These factors might influence the drilling-fluid-temperature profiles by incorporating the necessary heat/energy-system model as presented by Kumar et al. (2012a, b) for drilling operations, and for casing-while-drilling operations by including the plastering effect, as in Kumar and Samuel (2012).

Historically, many studies provided the necessary mathematical tools to describe the temperature distribution inside the wellbore. Earlier studies presented the basic analytical models and provided the physical understanding of the steady-state and transient-flow problems, as in Edwardson et al. (1962) and Tragesser et al. (1967). Raymond (1969) provided the first numerical model for computing circulating-fluid temperatures during unsteady- and pseudosteady-state conditions to handle multiple casing strings.

Furthermore, improvements to this model have been made by Keller et al. (1973) by adding new forms of energy as a result of frictional pressure losses throughout the drillpipe and annulus to the heat/energy system with the limitations of the provided data. This model was further investigated by Marshall and Bentsen (1982) using a full set of data. Subsequently, analytical solutions became feasible for less-complicated systems, such as that for a single casing string. For example, Holmes and Swift (1970) presented a solution for the steady-state heat transfer in a drillpipe and annulus surrounded by the formation. In contrast, Kabir et al. (1996) and Hasan et al. (1996) obtained solutions for forward- and reverse-circulation cases for a variable mud-tank temperature of the circulating fluid. Kumar and Samuel (2013) expanded the scope of the previous models by including well deviation and heat generated by wellbore friction. They validated their fluid-temperature model with field data involving deviated and horizontal wellbores.

The primary aim of this study is to offer a comparison between two analytical fluid-temperature models with two sources of energy. Initially, we considered the frictional heat that has been available for some time, and then one involving the rotational kinetic energy. Both of these models might influence the drillpipe- and annular-temperature profiles during different wellbore operations. We used limited field data to validate the performance of both models.

Mathematical Models

For completeness, this section presents models for two sources of energy: frictional energy (FE) and rotational kinetic energy (RKE). To gain clarity on the difference between these two models, see the schematic shown in **Fig. 1.** The heat generated from the RKE depends on the rotational speed of the drillstring, regardless of its physical contact with the wellbore. Consequently, the increase in fluid temperature will distribute gradually all around the drillstring. In contrast, the heat generated by frictional energy is caused by the contact points between the drillstring and the wellbore wall. Such contact might occur in some areas of the borehole in a vertical well, but more so when the well starts to deviate from vertical.

FE. Keller et al. (1973) suggested an analytical model of the heat/energy-balance system for determining the temperature profiles for both drillstring and annular temperature. The energy-system calculations are performed for steady-state and transient conditions using finite-difference equations for eight solution points in the presence of multiple casing strings. The calculations begin with the energy balance inside the drillstring and continue successively through the drillstring, the flow annulus, the first casing string, the second annulus, the third annulus, the fourth annulus, and into the formation. New energy sources added to the system involve the frictional flow in the drillpipe, wherein the shear work is performed by rotating the drillstring, and the frictional work at the drill bit. The validation of this model was performed by adopting the Holmes and Swift (1970) data.

Original SPE manuscript received for review 18 January 2018. Revised manuscript received for review 7 September 2018. Paper (SPE 194209) peer approved 22 September 2018.

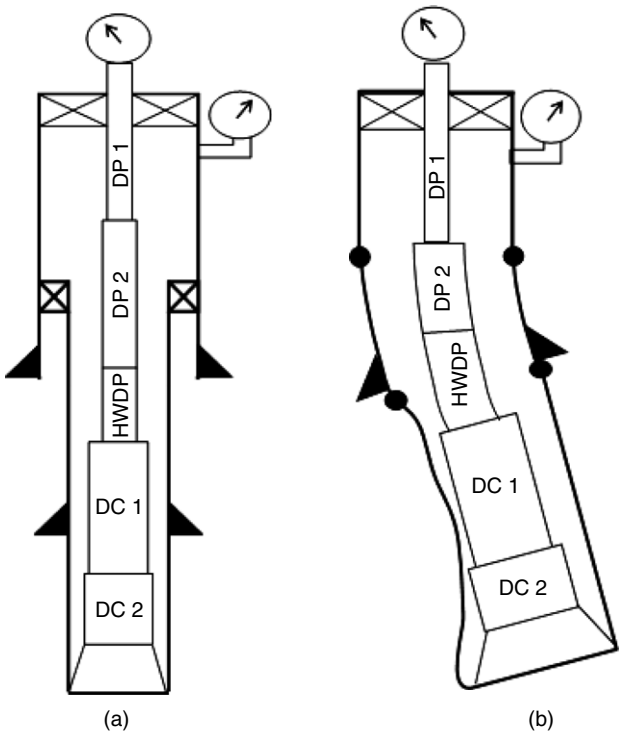

Fig. 1—Wellbore schematics: (a) vertical well; (b) deviated well. DC = drill collar; DP = drillpipe; HWDP = heavy-weight drillpipe.

Marshall and Bentsen (1982) further investigated the Keller et al. (1973) model using the entire data set required for the different casing sizes installed. Kumar and Samuel (2013) suggested a mathematical model for estimating the heat generated from the frictional forces of the drillstring and incorporated this model into an energy system to determine the final mathematical form that represents the drillpipe- and annular-temperature profiles. The energy system in this model was the same as that of Keller et al. (1973) and Marshall and Bentsen (1982), with one crucial difference. The Kumar and Samuel (2013) formulation presupposes that the steady-state heat transfer occurs from the drillpipe to the annulus and from the annulus to the adjacent formation.

The complete mathematical model for the Kumar and Samuel (2013) study did not appear in the paper, presumably for brevity. We attempted to fill in that perceived void in this study. For the steady-state condition, the mathematical forms of the energy-balance system for the annulus and the drillstring, respectively, can be expressed as

$$\rho q C_p \frac{\mathrm{d}T_a}{\mathrm{d}z} + 2\pi r_p U(T_{dp} - T_a) + 2\pi r_w h_o (T_f - T_a) + Q_a = 0, \quad \ldots\ldots (1)$$

$$\rho q C_p \frac{\mathrm{d}T_{dp}}{\mathrm{d}z} + 2\pi r_p U(T_{dp} - T_a) = Q_p. \quad \ldots\ldots (2)$$

Eq. 2 can be rewritten as

$$T_a = T_{dp} + \frac{\rho q C_p}{2\pi r_p U}\frac{\mathrm{d}T_{dp}}{\mathrm{d}z} - \frac{Q_p}{2\pi r_p U}. \quad \ldots\ldots (3)$$

The solution of the ordinary-differential equations (Eqs. 1 through 3) for the drillpipe temperature can be written as

$$T_{dpFE} = C_1 e^{r_1 z} + C_2 e^{r_2 z} + g_T z + T_S + \frac{Q_p}{2\pi r_p U} + \frac{Q_a + Q_p}{2\pi r_w h_o} - A g_T, \quad \ldots\ldots (4)$$

and for the annular temperature as

$$T_{aFE} = C_1(1 + Ar_1)e^{r_1 z} + C_2(1 + Ar_2)e^{r_2 z} + g_T z + T_S + \frac{Q_a + Q_p}{2\pi r_w h_o}, \quad \ldots\ldots (5)$$

where

$$A = \frac{\rho q C_p}{2\pi r_p U}. \quad \ldots\ldots (6)$$

The integration constants C_1 and C_2 can be found by applying the first kind of boundary condition (BC), or the Dirichlet BC. This BC implies that at the surface drillpipe temperature is the same as the inlet drillpipe temperature, whereas the annular and drillpipe temperatures are equal at total depth (TD), as given in Powers (2010). We note that this BC represents the industry standard, exemplified by Raymond (1969), Holmes and Swift (1970), Keller et al. (1973), Marshall and Bentsen (1982), Arnold (1990), Kumar and Samuel (2013), and Gao et al. (2017). With the Dirichlet BC, the two constants can be written as

$$C_2 = T_{dpi} - T_S - \frac{Q_p}{2\pi r_p U} - \frac{Q_a + Q_p}{2\pi r_w h_o} + Ag_T - C_1, \quad \ldots\ldots (7)$$

$$C_1 = \frac{\left[\left(T_{dpi} - T_S - \frac{Q_p}{2\pi r_p U} - \frac{Q_a + Q_p}{2\pi r_w h_o} + Ag_T\right) Ar_2 e^{r_2 L} - \frac{Q_p}{2\pi r_p U} + Ag_T\right]}{(Ar_2 e^{r_2 L} - Ar_1 e^{r_1 L})}. \quad \ldots\ldots (8)$$

Appendix A provides the details of these derivations.

RKE. Replacing the energy source in the proposed model with the energy sources caused by the RKE for both the annular and drillpipe temperature can be presented as

$$A\frac{dT_a}{dz} + (T_{dp} - T_a) + B(T_f - T_a) + R_{ra} = 0, \quad \ldots\ldots (9)$$

$$T_a = T_{dp} + A\frac{dT_{dp}}{dz} - R_{rp}, \quad \ldots\ldots (10)$$

where A is given by Eq. 6, and the other symbols are defined as

$$B = \frac{r_w h_o}{r_p U}, \quad \ldots\ldots (11)$$

$$R_{ra} = \frac{1.75\times10^{-8}(\rho_p A_p)(r_{po}^2 + r_{pi}^2) \times (R_s)^2}{(r_p U)t}, \quad \ldots\ldots (12)$$

$$R_{rp} = \frac{3.48\times10^{-8}(\rho_p A_{pi})(r_{pi}^2) \times (R_s)^2}{(r_p U)t}. \quad \ldots\ldots (13)$$

The final mathematical forms for the drillpipe and annular temperatures can be obtained from the solution of the ordinary-differential equations (Eqs. 9 and 10) as

$$T_{dpRKE} = C_a e^{r_1 z} + C_b e^{r_2 z} + g_T z + T_s + R_{rp} + \frac{R_{rp}}{B} + \frac{R_{ra}}{B} - Ag_T, \quad \ldots\ldots (14)$$

$$T_{aRKE} = C_a e^{r_1 z}(1 + Ar_1) + C_b e^{r_2 z}(1 + Ar_2) + T_s + g_T z + \frac{R_{rp}}{B} + \frac{R_{ra}}{B}, \quad \ldots\ldots (15)$$

where

$$C_a = T_{dpi} - T_s - R_{rp} - \frac{R_{rp}}{B} - \frac{R_{ra}}{B} + Ag_T - C_b, \quad \ldots\ldots (16)$$

$$C_b = \frac{\left[\left(T_{dpi} - T_s - R_{rp} - \frac{R_{rp}}{B} - \frac{R_{ra}}{B} + Ag_T\right) r_1 e^{r_1 L} - \frac{R_{rp}}{A} + g_T\right]}{(r_1 e^{r_1 L} - r_2 e^{r_2 L})}. \quad \ldots\ldots (17)$$

Appendix B presents the details of these derivations.

Verification of Models

The original model proposed by Keller et al. (1973) used the data set of a vertical wellbore presented by Holmes and Swift (1970). Using those data, we applied the FE model and the RKE model with assumed U and h_o values of 3.2 and 1 Btu/ft^2-hr-°F, respectively. The outputs of both models for the annular temperature, without including any bottomhole energy source, provide good agreement with that offered by Keller et al. (1973), as shown in **Fig. 2.** In this example, the RKE model shows the annular temperature to be approximately 1°F higher than the FE model at both well-bottom and surface conditions. The distributed energy presented by Fig. 2 refers to the data set from Keller et al. (1973).

Although the Holmes and Swift (1970) data indicated that all the properties are applicable for the entire well depth, circulation is the only assumption that can trigger the RKE model. Usually, no or low rotational speed of the drillstring might be applied to avoid stuck pipe. Therefore, we assumed 5 rev/min for 2 hours only. That is because, after tens of hours of mud circulation, the system will behave as though no energy source exists, thereby reflecting the steady-state circulation. To verify the proposed FE and RKE models, we adopted the data of Kumar and Samuel (2013) for the deviated well case, as shown in **Table 1.**

In this case, the drillstring stems from the bottom depth with an 8½-in. bit, measurement-while-drilling (MWD) tool, reamers, stabilizer, a rotary-steerable system, and 5-in. heavyweight drillpipe (HWDP). The kickoff depth was reported as true vertical depth (TVD) of 7,685 ft, followed by the buildup section at measured depth (MD) of 4,149 ft, and then extended with a tangent section at MD of 2,431 ft.

The Kumar and Samuel (2013) model was applied for the long tangent section from 11,834- to 14,265-ft TD by using 26 stands for 48 hours. On the basis of these data, the length of each stand equals 93.5 ft, the rate of penetration occurred at 50.64 ft/hr, and the time required to drill each stand was equal to 1.84 hours. These considerations collectively led to a high rotational speed used to drill this section. We used the data in Table 1 and assumed other data, such as flow rate of 210 gal/min or 1,685 ft^3/hr, mud density of 10.015 lbm/gal or 74.81 lbm/ft^3, T_{pi} of 102°F, $U = 2.5$ Btu/ft^2-hr-°F, and $h_o = 1.6$ Btu/ft^2-hr-°F. Some of these data came from the Marshall and Bentsen (1982) study. **Fig. 3** shows the results of the application of the FE model, the same output as from the Kumar and Samuel (2013) model.

The variation in the geothermal gradient along with MD was assumed using the formation temperature of offset wells. We emphasize that in all well-control calculations, especially for the pressure gradient, we used the TVD. Therefore, we assumed a different value

of geothermal gradient to match its variation after the kickoff-point depth. An approximate linear expression of $T_f = T_s + g_T \times z$ can represent the formation temperature of interest at a given depth. Calculations with the FE model then followed at each stand, leading to an inlet temperature for Stand 1 at 80.33°F and for Stand 26 at 107°F; **Fig. 4** presents these results.

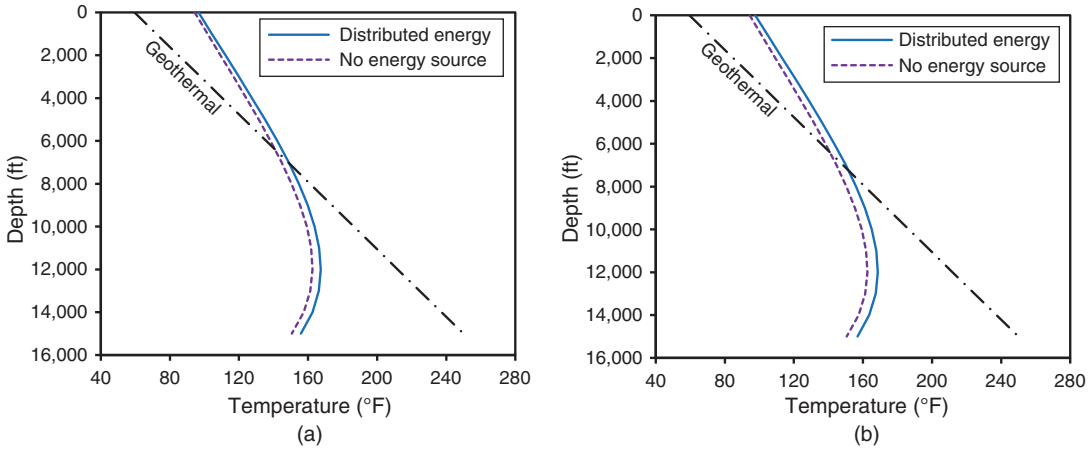

Fig. 2—Calculated annular temperature: (a) FE model; (b) RKE model. The term "distributed energy" refers to data from Keller et al. (1973).

Drilling Parameters	Values
Mud specific gravity	1.2
Plastic viscosity (cp)	20
Yield stress (lbm/100 ft^2)	15
Inlet temperature at drillpipe (°F)	80.33
Coefficient of friction in open hole	0.35
Surface temperature (°F)	59
Geothermal gradient (°F/ft)	0.013725
Openhole ID (in.)	8.5
Drillpipe OD (in.)	5
Drillpipe ID (in.)	3
Drillpipe weight (lbm/ft)	40
Drill collar OD (in.)	6.5
Drill collar ID (in.)	2.81
Drill collar length (ft)	520
Drill collar weight (lbm/ft)	100.8
Bit-nozzle total flow area (in^2)	1.2
Bit-nozzle velocity constant, C_d	0.95
Heat capacity of pipe/collar (Btu/lbm-°F)	0.0956
Thermal conductivity of pipe/collar (Btu/ft-hr-°F)	25.26

Table 1—Drilling parameters of Bingham plastic mud for a deviated well (Kumar and Samuel 2013). ID = inner diameter; OD = outer diameter.

The bottomhole temperature was measured from the bottom by 37 ft for MWD2 and 95 ft for MWD1. **Fig. 5** represents the result of applying the FE model for the annular temperature compared with the digitized temperature measurements for MWD1. The agreement between the digitized Kumar and Samuel (2013) model results and those from the FE model developed in this study is reassuring.

Now, let us consider two cases to verify the RKE model.

Case 1. In this case, we assumed that the heat generated from the RKE is added to the annular temperature only; that is, $Q_{rp} = 0$. We used the same data presented in Table 1, the same inlet temperature for the first and last stand at 80.33 and 107°F, respectively, and the same fluid properties with the constant rotational speed of 100 rev/min from Kumar et al. (2012a). The heat-transfer calculations from the formation to the annulus and then to the drillpipe presupposed $U = 3.6$ Btu/ft^2-hr-°F and $h_o = 1.5$ Btu/ft^2-hr-°F. The reported time required to drill this section was 48 hours; therefore, we started at 110 hours in the first stand, referring to all the previous operations until reaching this depth, and then increased the time for each stand until reaching 158 hours for Stand 26. **Fig. 6** shows the two temperature profiles of interest for the two stands.

Let us compare the results of the RKE model with the real-time temperature data while drilling. The calculated temperature trend appeared less than the MWD1 and MWD2, measurements resulting from the RKE in the annulus not being adequate to replace the FE sources, as suggested by Kumar and Samuel (2013). Moreover, applying the heat-energy model without accounting for the FE sources will result in a temperature that is approximately 20°F lower than with the inclusion of FE. **Fig. 7** presents the relevant results.

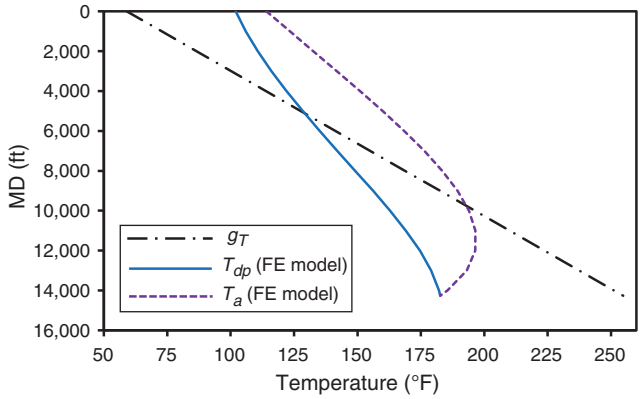

Fig. 3—Application of the FE model for the total depth.

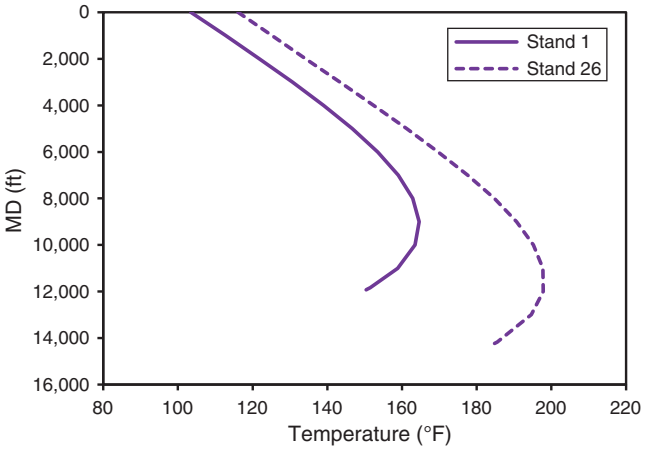

Fig. 4—Annular temperatures of the FE model for Stands 1 and 26.

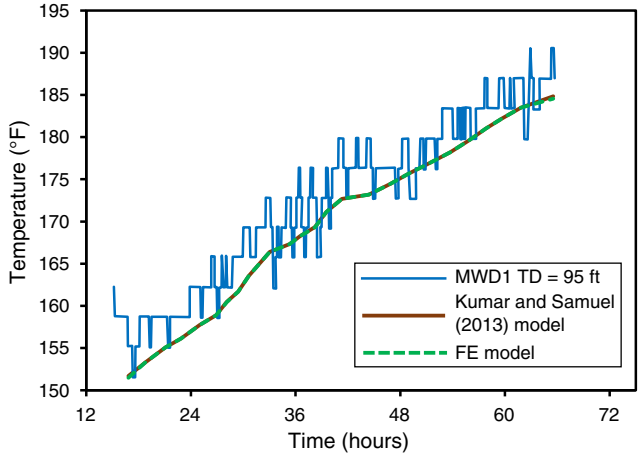

Fig. 5—Comparison of the FE model with the Kumar and Samuel (2013) model.

The drilling process in a deviated well provides a contact area of the drillstring with the wellbore, which might affect the value of the overall heat-transfer coefficient from the annulus to the drillpipe U. The overall heat-transfer coefficient from the formation to the annulus h_o remains constant with the steady-state assumption. Therefore, we retained the same data, and by changing U for each stand, we can obtain a good match with the measured data for MWD1 and MWD2. As shown in **Fig. 8,** invoking the RKE model causes a temperature difference of approximately 15°F.

We emphasize that the wellbore lacks uniformity as a result of the deviated-drilling operation, with an average inclination of approximately 10 to 11° in the tangent section. Therefore, the heat generated by frictional energy caused by the contact between the drillstring and the wellbore wall, as described by Kumar and Samuel (2013), might not occur uniformly on the inside area of the entire wellbore. In contrast, the application of RKE depends on the rotational speed of the drillstring, regardless of its contact with the wellbore. As a result, the temperature profiles from the RKE will be higher than the temperature profiles obtained by the FE model.

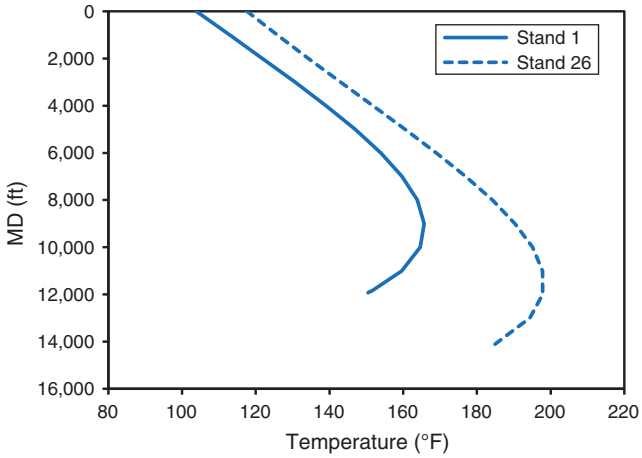

Fig. 6—Annular temperature of the RKE model for Stands 1 and 26.

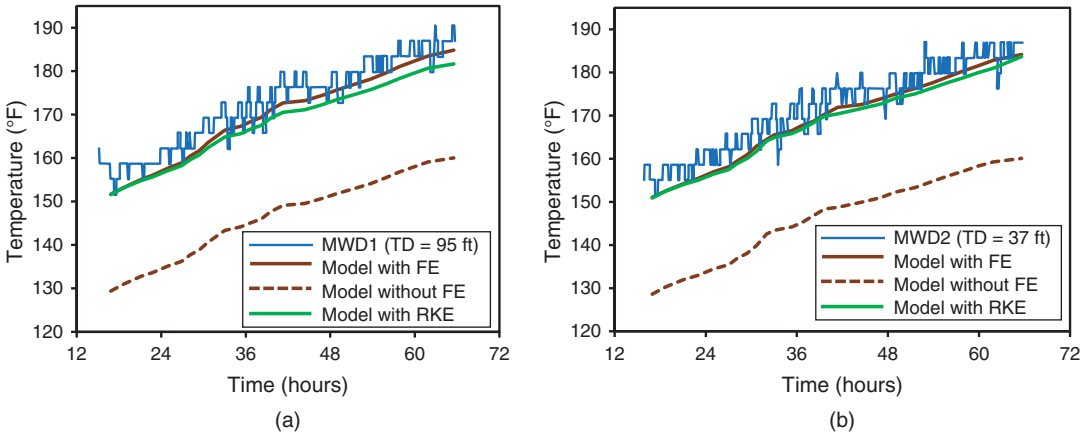

Fig. 7—Adding RKE to the annulus suggests a decent overall match with measured data: (a) MWD1; (b) MWD2.

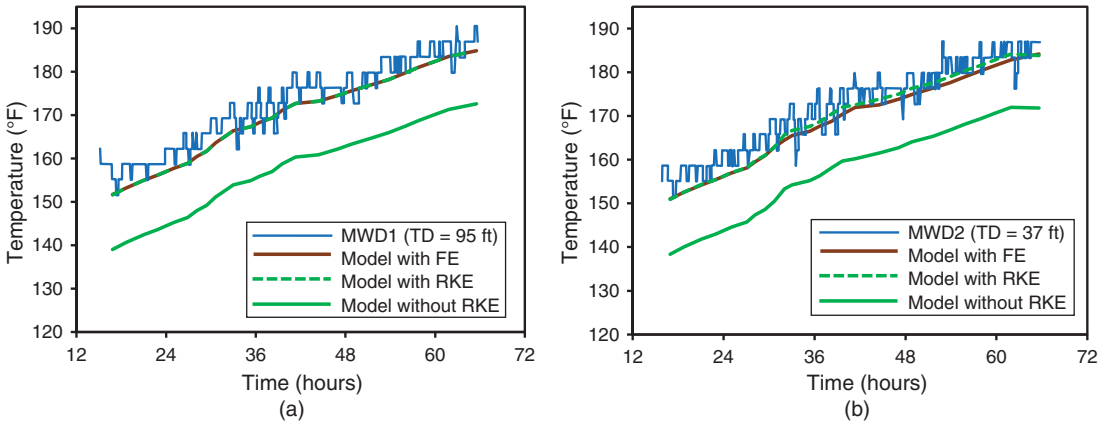

Fig. 8—Adding RKE to the annulus vs. measured data by changing *U*: (a) MWD1; (b) MWD2.

Case 2. In Case 2, the rotational energy working as the heat source can be added both to the fluid in the annulus Q_{ra} and to the drillpipe Q_{rp}, as given by the RKE model. The same data assumed in Case 1 were used to obtain an increase in temperature profile for each stand as a result of the new source added to the fluid inside the drillpipe, as given in **Figs. 9 and 10.**

Figs. 9 and 10 suggest that the amount of heat generated from the rotational energy inside the drillpipe was fully accounted for, which we refer to as the heat inside the drillpipe and from the drill bit. Therefore, one can assume that the heat source inside the drillpipe takes only 60% of the total generated heat, and the remaining 40% goes to the bit. Keller et al. (1973) initially suggested this assumption, which Marshall and Bentsen (1982) used. The use of this energy split will cause the annular-temperature profile to increase more than that in Case 1, and the comparison with the measured data suggests an improved match, as shown in **Fig. 11.**

Model Validation

We applied the proposed RKE model for 13 stands from 6,900- to 7,977-ft MD of a 12¼-in.-hole buildup section in a recently drilled deviated well. The required drilling time involved 53 hours, with the bottomhole assembly (BHA) consisting of a 12¼-in.

polycrystalline-diamond-compact bit, rotary-steerable system, MWD tool, 1×5-in. HWDP, drilling jar, and 7×5-in. HWDP. The temperature measurement was obtained using the MWD tool, located at 27 ft, which was the reference depth of measurement from the drill bit. Not all the required parameters for this field example were available; therefore, some required data were assumed from the literature. **Table 2** presents the drilling and fluid parameters, and **Table 3** presents drilling-measurement data.

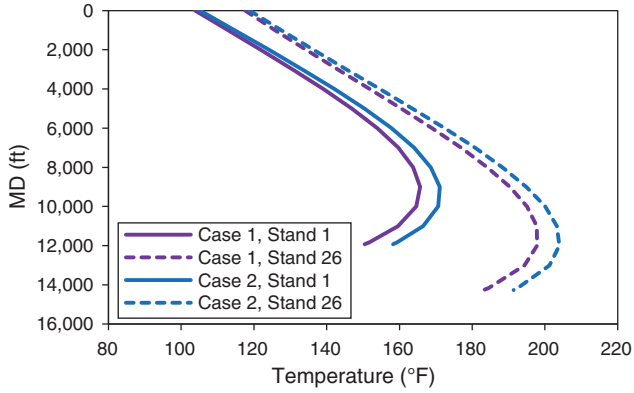

Fig. 9—Annular-temperature profiles in two stands derived from the RKE model.

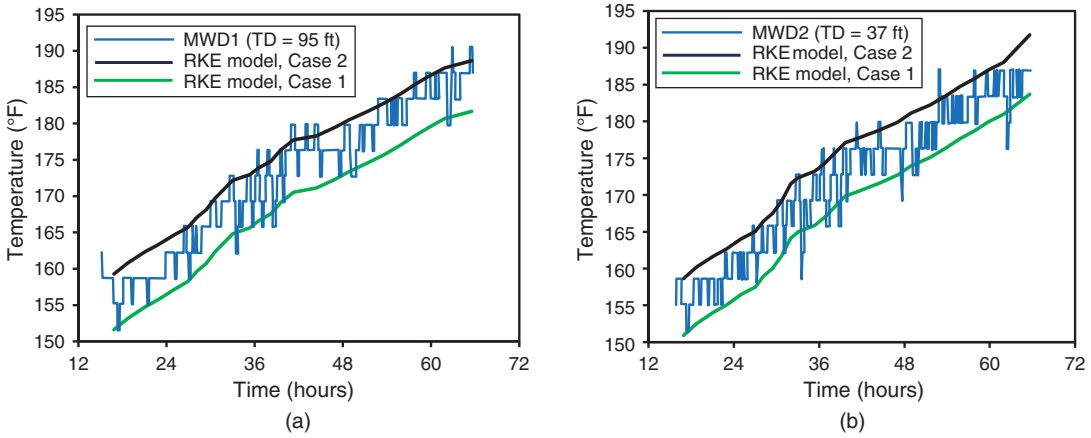

Fig. 10—Adding RKE to the annulus and drillstring vs. measured data: (a) MWD1; (b) MWD2.

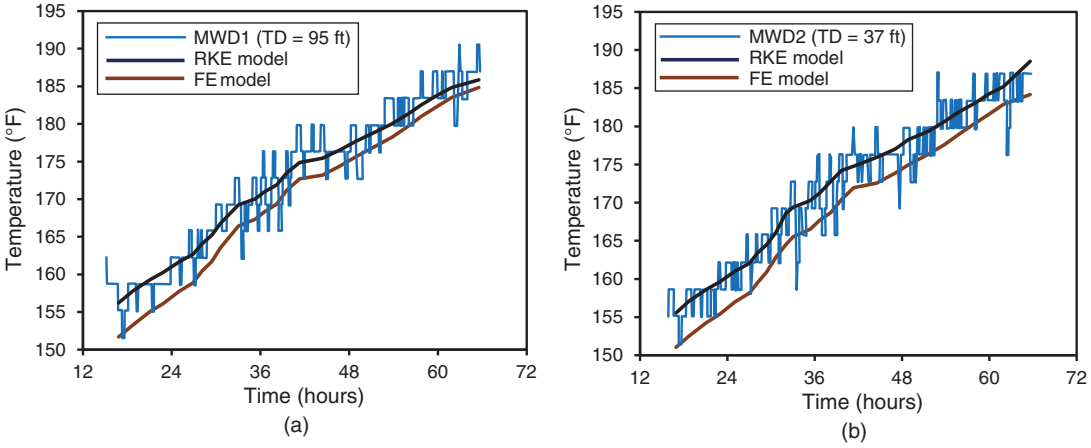

Fig. 11—Adding 60% of RKE to the drillstring shows good agreement with measured data at (a) MWD1; (b) MWD2.

We used the Hasan et al. (1996) model to estimate the required inlet-temperature data for this field case, given their unavailability. **Table 4** presents those estimated temperatures at each stand. The MWD tool provided the measured temperature; the assumed geothermal gradient of 0.013725°F/ft allowed conversion to the measurement depth. **Fig. 12** presents the application of the proposed RKE model for both the drillpipe temperature and the annular temperature.

Well and Mud Data	Values
Section depth (ft)	7,977
Drill-bit size (in.)	12¼
Drillstem OD (in.)	6⅝
Drillstem ID (in.)	3
Mud viscosity (cp)	21
Mud density (lbm/gal)	10.8
Circulation rate (gal/min)	750
Inlet-mud temperature (°F)	125
Formation density (lbm/gal)	20.86
Rotational speed (rev/min)	130
Section length (ft)	1,077

Table 2—Well and mud data. ID = inner diameter; OD = outer diameter.

Stand	Depth (ft)	Drilling Time (hours)	Inclination (degrees)	Azimuth (degrees)	TVD (ft)	Dogleg (°F/100 ft)	Vertical Section (ft)	Temperature (°F)
1	6,900	28.00	2.81	171.24	6,899.16	1.18	38.97	139.75
2	6,994	31.55	4.47	165.39	6,992.96	1.81	44.87	146.80
3	7,089	34.78	6.92	163.11	7,087.49	2.59	54.28	152.10
4	7,183	37.70	9.29	161.85	7,180.54	2.53	67.52	157.39
5	7,277	40.75	11.44	160.78	7,273.00	2.30	84.42	159.15
6	7,371	42.30	13.42	162.97	7,364.79	2.16	104.64	148.57
7	7,464	45.63	15.46	164.87	7,454.85	2.25	127.77	153.86
8	7,571	49.25	17.97	163.28	7,557.32	2.38	158.46	153.86
9	7,663	59.23	20.48	161.81	7,644.19	2.78	188.72	159.15
10	7,759	63.18	23.11	162.34	7,733.32	2.75	224.34	166.21
11	7,853	66.80	25.79	162.48	7,818.88	2.85	263.21	171.50
12	7,946	78.82	27.99	161.14	7,901.82	2.45	305.24	164.44
13	7,977	81.02	28.01	160.71	7,929.19	0.65	319.79	171.50

Table 3—Measured drilling data.

Stand	Depth (ft)	Inlet Temperature (°F)
1	6,900	125
2	6,994	132
3	7,089	140
4	7,183	146
5	7,277	149
6	7,371	137
7	7,464	143
8	7,571	143
9	7,663	152
10	7,759	160
11	7,853	166
12	7,946	160
13	7,977	167

Table 4—Estimated inlet temperature.

All temperature measurements recorded by the MWD tool occurred at MDs after the kickoff point. We can assume one value for the geothermal gradient for the vertical section only, although a variation in geothermal gradient might occur because of a change in sediments. Although not shown here, our findings suggest that the small differences in g_T produce insignificant results given the short drilling intervals.

By using the same field data given in Table 2 and the calculated inlet temperatures given by Table 4, we applied the FE model with Q_a and Q_p at 80 and 45 Btu/ft-hr, respectively. **Fig. 13** compares the model response with the measured temperature profiles for both the annulus and the drillpipe. The variation of the geothermal gradient produced no perceptible change in the model performance, similar to what was seen previously.

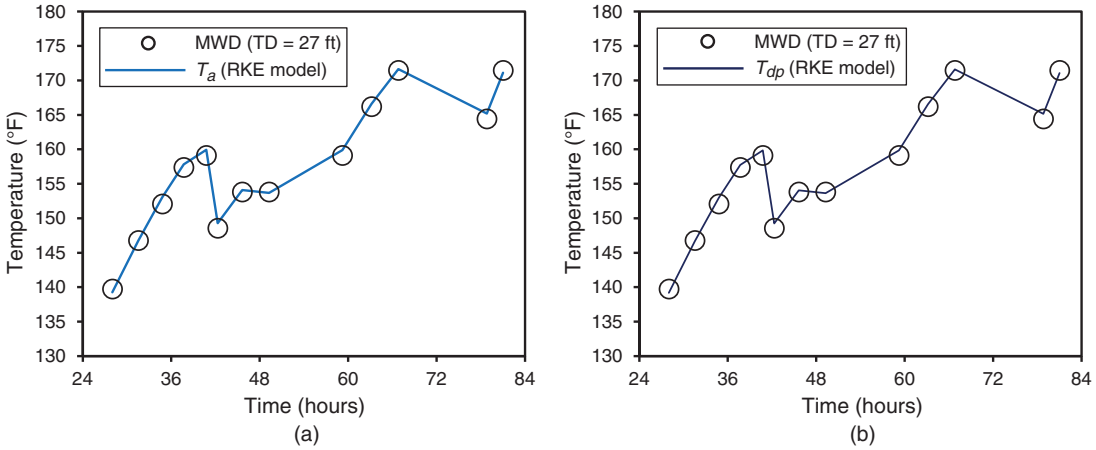

Fig. 12—Validation of the RKE model with MWD: (a) T_a; (b) T_{dp}.

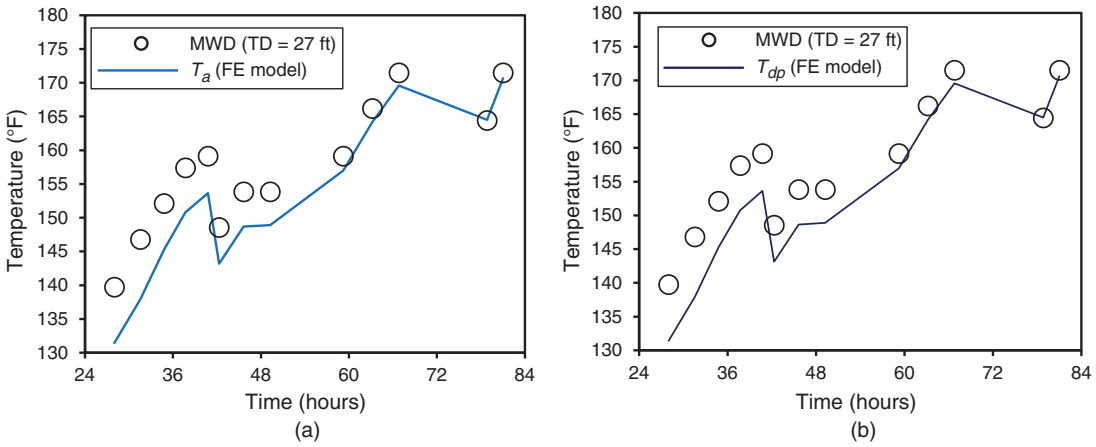

Fig. 13—Validation of the FE model with MWD: (a) T_a; (b) T_{dp}.

The heat generated by FE relates to the contact area between the drillstring and the wellbore, which depends on the survey measurement available at each depth. The inclination and azimuth gradually increase from the kickoff-point depth to the target depth. Also, at early drilling time, the directional survey is relatively smaller than the late-time survey measurements. Therefore, heat generated at earlier times becomes insufficient to match the MWD measurements. In contrast, at late drilling times, the drilling-survey measurement will show more contact area required for generating the heat added to the drilling fluid, which could explain the improved match with the MWD measurements.

Discussion

The primary objective of this paper was the investigation of the sources of energy that might affect temperature profiles in both mud conduits in a drilling operation. To that end, we have explored development and applications of both FE and RKE models. Analytical formulation underpins both models. The amount of rotational energy depends on the type of technology used in drilling. The prospect of these models provides some new insights that could be included in future studies in challenging environments.

The heat generated from the FE resulting from the frictional force contact between the drillstring and the wellbore was assumed to be constant along the entire wellbore depth. This underlying assumption could be open to debate because the actual contact occurs in some areas of the borehole in a vertical or nearly vertical setting. However, in deviated wells, this assumption becomes a reality, as high torque readings will suggest. In contrast, the RKE depends on the rotating speed of the drillstring, regardless of the physical contact with the formation. Therefore, the temperature profiles generated with the RKE model will be higher than those produced with the FE model. We also note that the variation between TVD and MD, as a result of directional drilling, might lead to a change in geothermal gradient. However, this difference is likely to be small because of the short length of the drilling interval.

Validation of the proposed models with field data supports the application of the rotating energy. The RKE caused by rotation of the drillstring was assumed in two cases (Cases 1 and 2) and was presented previously to cover all possible temperature ranges in a typical drilling operation. The performance of the model when compared with the drillpipe- and annular-temperature data provided confidence in the solution approach pursued in this study.

One can observe that the results of the FE and RKE models appear similar for the problems discussed here despite their different formulations. During a drilling operation, temperature measurement can be obtained by the MWD sensor, which is usually at least 30 ft above the drill bit, followed by the BHA. Therefore, in a deviated well, the contact area with the formation by the BHA promotes thermal energy caused by friction, leading to the proper application of the FE model; a similar situation might arise while encountering a tight spot in a vertical well. Of course, frictional energy becomes the primary driver while drilling a horizontal well. In contrast, the RKE model depends only on the rotation of the drillstring, which occurs continuously through all operations, regardless of the well deviation.

We note that the BC (condition of the first kind or Dirichlet condition) used in the solution of the FE and RKE models leads to the reported results. However, a different set of results will appear when the BCs differ. For instance, if we assume the Neumann condition

($dT_a/dz = 0$ at $z = L$) or the Robin condition ($dT_t/dz|_{z=0} = dT_t/dz|_{z=L} = 0$) to solve the fundamental equations, then increased temperature profiles occur in both conduits. Al Saedi et al. (2018) made this point.

Conclusions

Our conclusions from this text are the following:

1. This study presents a new analytical model involving the RKE, which can be included in any energy-balance system of equations, fluid-temperature profiles during drilling, and fluid-circulation operations in the wellbore.
2. This study also explored the development and use of the FE model (Kumar and Samuel 2013) to generate the temperature profiles in a drilling operation. In general, the RKE model tends to produce somewhat-higher temperature profiles than the FE model, as field data suggest.
3. The maximum temperature occurs at a depth above the well bottom for both models. This outcome is a consequence of the use of the first kind of BC, or Dirichlet condition. Field examples suggested that both the FE model and the RKE model tend to produce the necessary energy needed to replicate the field measurements. They appear case dependent; therefore, both of them merit consideration while estimating temperature profiles.

Nomenclature

A = parameter defined by Eq. 6, ft
A_p = outer-drillpipe area, ft^2
A_{pi} = inner-drillpipe area, ft^2
B = parameter defined by Eq. B-20, dimensionless
C_a = integration constant defined by Eq. B-28, °F
C_b = integration constant defined by Eq. B-30, °F
C_d = bit-nozzle-velocity constant
C_p = heat capacity of mud, Btu/lbm-°F
C_1 = integration constant defined by Eq. A-18, °F
C_2 = integration constant defined by Eq. A-16, °F
f = frequency, rev/sec
g_T = geothermal gradient, °F/ft
h_o = overall heat-transfer coefficient across wellbore wall, Btu/ft^2-°F-hr
I = moment of inertia, lbm-ft^2
K_E = kinetic energy, lbm-ft^2/sec^2
L = TD (MD), ft
m_p = tubular mass, lbm
N = parameter defined by Eq. A-9, °F
q = mud-flow rate, ft^3/hr
Q_a = heat source in annulus, Btu/ft-hr
Q_{fa} = heat flow from formation to annulus, Btu/ft-hr
Q_p = heat source inside drillstring, Btu/ft-hr
Q_{pa} = heat flow from pipe to annulus, Btu/ft-hr
Q_{ra} = heat source in annulus caused by rotational energy, Btu/hr
Q_{rp} = heat source inside drillstring caused by rotational energy, Btu/hr
r_1, r_2 = exponent coefficients defined by Eq. A-10, ft^{-1}
r_p = outer radius of the drillstring, ft
r_{pi} = average inner radius of the drillstring, ft
r_{po} = average outer radius of the drillstring, ft
r_w = wellbore radius, ft
R_{ra} = parameter defined by Eq. B-21, °F
R_{rp} = parameter defined by Eq. B-14, °F
R_s = rotating speed, rev/min
t = drilling or circulation time, hours
T_a = mud temperature in annulus, °F
T_{aFE} = annular fluid temperature by frictional energy, °F
T_{aRKE} = annular fluid temperature by rotational kinetic energy, °F
T_{dp} = temperature of drillstring fluid, °F
T_{dpc} = complementary solution for drillstring fluid temperature, °F
T_{dpi} = inlet fluid temperature, °F
T_{dpp} = particular solution for drillstring fluid temperature, °F
T_{dpFE} = drillstring fluid temperature by frictional energy, °F
T_{dpRKE} = drillstring fluid temperature by rotational kinetic energy, °F
T_f = formation temperature, °F
T_{pi} = inlet fluid temperature, °F
T_s = surface temperature of Earth, °F
U = overall heat-transfer coefficient across drillpipe, Btu/ft^2-°F-hr
W = angular velocity, rad/sec
z = any vertical-well depth, ft
ρ = drilling-fluid density, lbm/ft^3
ρ_p = drillpipe density, lbm/ft^3

Acknowledgment

Author A. Q. Al Saedi gratefully acknowledges the financial support provided by the Higher Committee for Education Development in Iraq in pursuit of his PhD-degree study.

References

Aadnoy, B. S. and Djurhuus, J. 2008. Theory and Application of a New Generalized Model for Torque and Drag. Presented at the IADC/SPE Asia Pacific Drilling Technology Conference and Exhibition, Jakarta, Indonesia, 25–27 August. SPE-114684-MS. https://doi.org/10.2118/114684-MS.

Aadnoy, B. S., Fazaelizadeh, M., and Hareland, G. 2010. A 3D Analytical Model for Wellbore Friction. *J Can Pet Technol* **49** (10): 25–36. SPE-141515-PA. https://doi.org/10.2118/141515-PA.

Al Saedi, A. Q., Flori, R. E., and Kabir, C. S. 2018. New Analytical Solutions of Wellbore Fluid Temperature Profiles During Drilling, Circulating, and Cementing Operations. *J. Pet. Sci. Eng.* **170** (November): 206–217. https://doi.org/10.1016/j.petrol.2018.06.027.

Arnold, F. C. 1990. Temperature Variation in a Circulating Wellbore Fluid. *J Energy Resour. Technol.* **112** (2): 79–83. https://doi.org/10.1115/1.2905726.

Edwardson, M. J., Girner, H. M., Parkison, H. R. et al. 1962. Calculation of Formation Temperature Disturbances Caused by Mud Circulation. *J Pet Technol* **14** (4): 416–426. SPE-124-PA. https://doi.org/10.2118/124-PA.

Gao, Y., Sun, B., Xu, B. et al. 2017. A Wellbore/Formation-Coupled Heat-Transfer Model in Deepwater Drilling and Its Application in the Prediction of Hydrate-Reservoir Dissociation. *SPE J.* **22** (3): 756–766. SPE-184398-PA. https://doi.org/10.2118/184398-PA.

Giancoli, D. C. 2013. *Physics for Scientists and Engineers With Modern Physics*, Vol. 3. London: Pearson Education.

Hasan, A. R., Kabir, C. S., and Ameen, M. M. 1996. A Fluid Circulating Temperature Model for Workover Operations. *SPE J.* **1** (2): 133–144. SPE-27848-PA. https://doi.org/10.2118/27848-PA.

Holmes, C. S. and Swift, S. C. 1970. Calculation of Circulating Mud Temperatures. *J Pet Technol* **22** (6): 670–674. SPE-2318-PA. https://doi.org/10.2118/2318-PA.

Kabir, C. S., Hasan, A. R., Kouba, G. E. et al. 1996. Determining Circulating Fluid Temperature in Drilling, Workover, and Well Control Operations. *SPE Drill & Compl* **11** (2): 74–79. SPE-24581-PA. https://doi.org/10.2118/24581-PA.

Keller, H. H., Couch, E. J., and Berry, P. M. 1973. Temperature Distribution in Circulating Mud Columns. *SPE J.* **13** (1): 23–30. SPE-3605-PA. https://doi.org/10.2118/3605-PA.

Kumar, A. and Samuel, R. 2012. Analytical Model to Estimate the Downhole Temperatures for Casing While Drilling Operations. Presented at the SPE Annual Technical Conference and Exhibition, San Antonio, Texas, 8–10 October. SPE-159278-MS. https://doi.org/10.2118/159278-MS.

Kumar, A. and Samuel, R. 2013. Analytical Model to Predict the Effect of Pipe Friction on Downhole Fluid Temperatures. *SPE Drill & Compl* **28** (3): 270–277. SPE-165934-PA. https://doi.org/10.2118/165934-PA.

Kumar, A., Singh, A. P., and Samuel, R. 2012a. Analytical Model to Predict the Effect of Pipe Friction on Downhole Temperatures for Extended Reach Drilling (ERD). Presented at the IADC/SPE Drilling Conference and Exhibition, San Diego, California, 6–8 March. SPE-151254-MS. https://doi.org/10.2118/151254-MS.

Kumar, A., Singh, A. P., and Samuel, R. 2012b. Field Application of an Analytical Model for Estimating the Downhole Temperatures Due to Wellbore Friction. Presented at the IADC/SPE Asia Pacific Drilling Technology Conference and Exhibition, Tianjin, China, 9–11 July. SPE-156307-MS. https://doi.org/10.2118/156307-MS.

Marshall, D. W. and Bentsen, R. G. 1982. A Computer Model to Determine the Temperature Distributions in a Wellbore. *J Can Pet Technol* **21** (1): 63–75. PETSOC-82-01-05. https://doi.org/10.2118/82-01-05.

Mirhaj, S. A., Kaarstad, E., and Aadnoy, B. S. 2016. Torque and Drag Modeling; Soft-String vs. Stiff-String Models. Presented at the SPE/IADC Middle East Drilling Technology Conference and Exhibition, Abu Dhabi, 26–28 January. SPE-178197-MS. https://doi.org/10.2118/178197-MS.

Powers, D. L. 2010. *Boundary Value Problems and Partial Differential Equations*. Amsterdam: Academic Press.

Raymond, L. 1969. Temperature Distribution in a Circulating Drilling Fluid. *J Pet Technol* **21** (3): 333–341. SPE-2320-PA. https://doi.org/10.2118/2320-PA.

Samuel, G. R. 2007. *Downhole Drilling Tools: Theory and Practice for Engineers and Students*. Houston: Gulf Publishing Company.

Tragesser, A. F., Crawford, P. B., and Crawford, H. R. 1967. A Method for Calculating Circulating Temperatures. *J Pet Technol* **19** (11): 1507–1712. SPE-1484-PA. https://doi.org/10.2118/1484-PA.

Appendix A—FE Model

The assumptions and all the mathematical details of this model were presented by Kumar and Samuel (2013). Application of the energy balance for the steady-state condition leads to the differential form of the forward circulation in a drillpipe, which is given by

$$\rho q C_p \frac{\mathrm{d}T_{dp}}{\mathrm{d}z} + 2\pi r_p U(T_{dp} - T_a) = Q_p, \quad \text{(A-1)}$$

or

$$T_a = T_{dp} + \frac{\rho q C_p}{2\pi r_p U}\frac{\mathrm{d}T_{dp}}{\mathrm{d}z} - \frac{Q_p}{2\pi r_p U}. \quad \text{(A-2)}$$

Differentiating Eq. A-2, we obtain

$$\frac{\mathrm{d}T_a}{\mathrm{d}z} = \frac{\mathrm{d}T_{dp}}{\mathrm{d}z} + \frac{\rho q C_p}{2\pi r_p U}\frac{\mathrm{d}^2 T_{dp}}{\mathrm{d}z^2}, \quad \text{(A-3)}$$

and for the annulus,

$$\rho q C_p \frac{\mathrm{d}T_a}{\mathrm{d}z} + 2\pi r_p U(T_{dp} - T_a) + 2\pi r_w h_o (T_f - T_a) + Q_a = 0. \quad \text{(A-4)}$$

Substituting Eqs. A-2 and A-3 into Eq. A-4 and simplifying, and considering $T_f = T_s + g_T \times z$, we obtain

$$\frac{(\rho q C_p)^2}{2\pi r_p U}\frac{\mathrm{d}^2 T_{dp}}{\mathrm{d}z^2} - 2\pi r_w h_o \frac{\rho q C_p}{2\pi r_p U}\frac{\mathrm{d}T_{dp}}{\mathrm{d}z} - 2\pi r_w h_o T_{dp} = -2\pi r_w h_o T_s - 2\pi r_w h_o g_T z - 2\pi r_w h_o \frac{Q_p}{2\pi r_p U} - Q_p - Q_a. \quad \text{(A-5)}$$

The solution of the left-hand side of Eq. A-5, which represents the homogeneous (complementary) part, is given by

$$T_{dpc} = C_1 e^{r_1 z} + C_2 e^{r_2 z}. \quad \text{(A-6)}$$

The right-hand side of Eq. A-5 refers to the particular part, and its solution is given by

$$T_{dpp} = g_T z + N. \quad \text{(A-7)}$$

Therefore, the final solution of Eq. A-5 can be obtained by summation of Eqs. A-6 and A-7, which is given by

$$T_{dp} = C_1 e^{r_1 z} + C_2 e^{r_2 z} + g_T z + N, \quad \text{(A-8)}$$

where

$$N = T_S + \frac{Q_a + Q_p}{2\pi r_w h_o} + \frac{[Q_p - (\rho q C_p) g_T]}{2\pi r_p U} \quad \text{(A-9)}$$

and

$$r_1, r_2 = \frac{(2\pi r_w h_o) \pm \sqrt{(2\pi r_w h_o)^2 + 4(2\pi r_p U)(2\pi r_w h_o)}}{2\rho q C_p}. \quad \text{(A-10)}$$

Eq. A-8 can be rewritten as

$$T_{dpFE} = C_1 e^{r_1 z} + C_2 e^{r_2 z} + g_T z + T_S + \frac{Q_p}{2\pi r_p U} + \frac{Q_a + Q_p}{2\pi r_w h_o} - A g_T, \quad \text{(A-11)}$$

$$A = \frac{\rho q C_p}{2\pi r_p U}. \quad \text{(A-12)}$$

Differentiating Eq. A-11, we obtain

$$\frac{\mathrm{d}T_{dp}}{\mathrm{d}z} = r_1 C_1 e^{r_1 z} + r_2 C_2 e^{r_2 z} + g_T. \quad \text{(A-13)}$$

Substituting Eqs. A-11 and A-13 into Eq. A-2 and simplifying, we obtain

$$T_{aFE} = C_1(1 + A r_1) e^{r_1 z} + C_2(1 + A r_2) e^{r_2 z} + g_T z + T_S + \frac{Q_a + Q_p}{2\pi r_w h_o}. \quad \text{(A-14)}$$

To find the integration constants C_1 and C_2, we need to apply the first kind of the BC (or the Dirichlet BC), as discussed after Eq. 6, as follows.

At surface, $z = 0$ and $T_{dp} = T_{dpi}$; therefore Eq. A-11 is given as

$$T_{dpi} = C_1 + C_2 + T_S + \frac{Q_p}{2\pi r_p U} + \frac{Q_a + Q_p}{2\pi r_w h_o} - A g_T, \quad \text{(A-15)}$$

$$C_2 = T_{dpi} - T_S - \frac{Q_p}{2\pi r_p U} - \frac{Q_a + Q_p}{2\pi r_w h_o} + A g_T - C_1. \quad \text{(A-16)}$$

At well TD or $z = L$, $T_{dpL} = T_{aL}$, and Eqs. A-11 and A-14 are given as

$$A r_1 C_1 e^{r_1 L} + A r_2 C_2 e^{r_2 L} = \frac{Q_p}{2\pi r_p U} - A g_T. \quad \text{(A-17)}$$

Substituting Eq. A-16 into Eq. A-17 and simplifying, we obtain

$$C_1 = \frac{\left[\left(T_{dpi} - T_S - \frac{Q_p}{2\pi r_p U} - \frac{Q_a + Q_p}{2\pi r_w h_o} + A g_T\right) A r_2 e^{r_2 L} - \frac{Q_p}{2\pi r_p U} + A g_T\right]}{(A r_2 e^{r_2 L} - A r_1 e^{r_1 L})}. \quad \text{(A-18)}$$

Appendix B—RKE Model

The kinetic energy of a rotating object is analogous to linear kinetic energy and can be expressed by the moment of inertia and angular velocity. During a drilling operation, the total kinetic energy resulting from the rotation of the drillstring can be transferred to two kinds of heat source added to the drilling fluid inside the drillstring (Q_{rp}) and in the annulus (Q_{ra}). Giancoli (2013) provides the RKE, which is given by

$$K_E = \frac{1}{2} \times I \times W^2, \quad \text{(B-1)}$$

where I refers to the moment of inertia (in lbm-ft^2) and W is the angular velocity (in rad/sec). Then, the moment of inertia can be calculated for the annulus as

$$I = \frac{m_p}{2}\left(r_{po}^2 + r_{pi}^2\right), \quad \text{(B-2)}$$

$$I = \frac{\rho_p \times (A \times \mathrm{d}z)_p}{2}\left(r_{po}^2 + r_{pi}^2\right), \quad \text{(B-3)}$$

where r_{po} and r_{pi} sequentially represent the tubular outer diameter (OD) and inner diameter (ID) (in ft) and m refers to the tubular mass (in lbm).

For the angular velocity, $W = \text{cycle} \times f$, where f is the frequency or rev/min in drilling; by converting rev/min to rev/sec,

$$f|_{\text{sec}} = R_s = \text{rev/min} = \frac{\text{rev}}{\text{min}} \times \frac{\text{min}}{60 \text{ seconds}} = \frac{\text{rev}}{60 \text{ seconds}}. \quad \text{(B-4)}$$

One cycle of any tubular will be equal to 2π/rev. Thus, the angular velocity will be equal to

$$W = \frac{2\pi \times R_s}{60}, \quad \text{(B-5)}$$

where W is in rad/sec. Now, after calculating the angular velocity and the moment of inertia, the kinetic energy in Eq. B-1 can be rewritten as

$$Q_{ra} = K_E = \frac{1}{2} \times \frac{\rho_p \times (A_p \times \mathrm{d}z)}{2}\left(r_{po}^2 + r_{pi}^2\right) \times \left(\frac{2\pi \times R_s}{60}\right)^2. \quad \text{(B-6)}$$

Eq. B-6 represents the total RKE transferred to heat in the annulus (in lbm-ft^2/sec^2). By converting this energy to Btu and dividing Eq. B-6 by the total time for drilling or circulating, we obtain the final mathematical form as

$$Q_{ra} = \frac{(1.098 \times 10^{-7})\rho_p \times (A_p \times \mathrm{d}z)\left(r_{po}^2 + r_{pi}^2\right) \times (R_s)^2}{t}, \quad \text{(B-7)}$$

where Q_{ra} represents the amount of heat added to the inside of the annulus system as a result of rotation of the drillstring (in Btu/hr), and t is the total drilling or circulating time (in hours). The heat added to the inside of the drillstring as a result of rotating the drillstring Q_{rp} is given by

$$Q_{rp} = \frac{(2.2 \times 10^{-7})\rho_p \times (A_{pi} \times \mathrm{d}z)\left(r_{pi}^2\right) \times (R_s)^2}{t}. \quad \text{(B-8)}$$

The difference between Eqs. B-7 and B-8 is because of the change in the moment of inertia for the inside of the drillstring, given as $I = \rho_p \times (A_p \times \mathrm{d}z)(r_{pi}^2)$.

Replacing the heat sources in the energy system in Appendix A with the new heat source suggested by RKE provides a new analytical model to determine the fluid-temperature behavior in the drillpipe and annulus. The heat source added to the system by the RKE is Q_{rp} and Q_{ra} (in Btu/hr). In contrast, the heat source in Keller et al. (1973), Marshall and Bentsen (1982), and Kumar and Samuel (2013) has a different unit, Btu/ft-hr.

Therefore, we need to rederive the energy system proposed in Appendix A in the following manner. The heat-energy balance for the steady-state condition in the drillpipe is given by

$$Q_{p(z)} - Q_{p(z+\mathrm{d}z)} - Q_{pa} + Q_{rp} = 0. \quad \text{(B-9)}$$

Substituting each term in Eq. B-9, we obtain

$$\rho q C_p\left(T_{dp(z)} - T_{dp(z+\mathrm{d}z)}\right) - 2\pi r_p U(T_{dp} - T_a)\mathrm{d}z + \frac{2.2 \times 10^{-7}\left(\rho_p A_p \mathrm{d}z\right)\left(r_{pi}^2\right) \times (R_s)^2}{t} = 0. \quad \text{(B-10)}$$

Simplifying Eq. B-10 as

$$\frac{\rho q C_p}{2\pi r_p U}\frac{\mathrm{d}T_{dp}}{\mathrm{d}z} + (T_{dp} - T_a) - \frac{2.2 \times 10^{-7}\left(\rho_p A_p\right)\left(r_{pi}^2\right) \times (R_s)^2}{2\pi r_p U t} = 0, \quad \text{(B-11)}$$

or

$$T_a = T_{dp} + A\frac{\mathrm{d}T_{dp}}{\mathrm{d}z} - R_{rp}, \quad \text{(B-12)}$$

where

$$A = \frac{\rho q C_p}{2\pi r_p U} \quad \text{(B-13)}$$

and

$$R_{rp} = \frac{3.48 \times 10^{-8}\left(\rho_p A_p\right)\left(r_{pi}^2\right) \times (R_s)^2}{r_p U t}. \quad \text{(B-14)}$$

Differentiating Eq. B-12, we obtain

$$\frac{dT_a}{dz} = \frac{dT_{dp}}{dz} + A\frac{d^2T_{dp}}{dz^2}. \quad \text{(B-15)}$$

The mathematical form of the annular energy balance is given by

$$Q_{a(z+dz)} - Q_{a(z)} + Q_{pa} + Q_{fa} + Q_{ra} = 0. \quad \text{(B-16)}$$

Eq. B-16 with the mathematical representation of each term can be written as

$$\rho q C_p\left(T_{a(z+dz)} - T_{a(z)}\right) + 2\pi r_p U(T_{dp} - T_a)dz + 2\pi r_w h_o(T_f - T_a)dz + \frac{1.098\times10^{-7}(\rho_p A_p dz)\left(r_{po}^2 + r_{pi}^2\right)\times(R_s)^2}{t} = 0. \quad \text{(B-17)}$$

Rearranging Eq. B-17,

$$\frac{\rho q C_p}{2\pi r_p U}\frac{\left(T_{a(z+dz)} - T_{a(z)}\right)}{dz} + (T_{dp} - T_a) + \frac{2\pi r_w h_o}{2\pi r_p U}(T_f - T_a) + \frac{1.098\times10^{-7}(\rho_p A_p)\left(r_{po}^2 + r_{pi}^2\right)\times(R_s)^2}{2\pi r_p U t} = 0, \quad \text{(B-18)}$$

or

$$A\frac{dT_a}{dz} + (T_{dp} - T_a) + B(T_f - T_a) + R_{ra} = 0 \quad \text{(B-19)}$$

where

$$B = \frac{r_w h_o}{r_p U} \quad \text{(B-20)}$$

and

$$R_{ra} = \frac{1.75\times10^{-8}\rho_p A_p\left(r_{po}^2 + r_{pi}^2\right)\times(R_s)^2}{r_p U t}. \quad \text{(B-21)}$$

Substituting Eqs. B-12 and B-15 into Eq. B-19 and simplifying, and considering $T_f = T_s + g_T \times z$, we obtain

$$A^2\frac{d^2T_{dp}}{dz^2} - AB\frac{dT_{dp}}{dz} - BT_{dp} = -BT_f - BR_{rp} - R_{rp} - R_{ra}. \quad \text{(B-22)}$$

The summation of the homogeneous and inhomogeneous solutions of the second-order ordinary-differential equation (Eq. B-22) leads to

$$T_{dpRE} = C_a e^{r_1 z} + C_b e^{r_2 z} + g_T z + T_s + R_{rp} + \frac{R_{rp}}{B} + \frac{R_{ra}}{B} - Ag_T, \quad \text{(B-23)}$$

where

$$r_1, r_2 = \frac{B}{2A}\left(1 \pm \sqrt{1 + \frac{4}{B}}\right). \quad \text{(B-24)}$$

Differentiating Eq. B-23, we obtain

$$\frac{dT_{dp}}{dz} = r_1 C_a e^{r_1 z} + r_2 C_b e^{r_2 z} + g_T. \quad \text{(B-25)}$$

Substituting Eqs. B-24 and B-23 into Eq. B-12 and simplifying yields

$$T_{aRE} = C_a e^{r_1 z}(1 + Ar_1) + C_b e^{r_2 z}(1 + Ar_2) + T_s + g_T z + \frac{R_{rp}}{B} + \frac{R_{ra}}{B}, \quad \text{(B-26)}$$

and C_a and C_b depend on the Dirichlet BC, at surface depth or $z = 0$, and $T_{dp} = T_{dpi}$. Justification of the Dirichlet BC is discussed after Eq. 6. Eq. B-23 can be written as

$$T_{dpi} = C_a + C_b + T_s + R_{rp} + \frac{R_{rp}}{B} + \frac{R_{ra}}{B} - Ag_T, \quad \text{(B-27)}$$

or

$$C_a = T_{dpi} - T_s - R_{rp} - \frac{R_{rp}}{B} - \frac{R_{ra}}{B} + Ag_T - C_b. \quad \text{(B-28)}$$

At well TD or $z = L$, $T_{dpL} = T_{aL}$, and Eqs. B-23 and B-25 yield

$$Ar_1C_ae^{r_1L} + Ar_2C_be^{r_2L} = R_{rp} - Ag_T. \quad \text{(B-29)}$$

Substituting Eq. B-28 into Eq. B-29 and simplifying, we obtain

$$C_b = \frac{\left[\left(T_{dpi} - T_s - R_{rp} - \frac{R_{rp}}{B} - \frac{R_{ra}}{B} + Ag_T\right)r_1e^{r_1L} - \frac{R_{rp}}{A} + g_T\right]}{(r_1e^{r_1L} - r_2e^{r_2L})}. \quad \text{(B-30)}$$

Ahmed Qasim Al Saedi is a PhD-degree candidate in petroleum engineering in the Geosciences and Geological and Petroleum Engineering Department at Missouri University of Science and Technology. His research interests include wellbore-temperature modeling and transient well testing. Al Saedi previously worked as a drilling supervisor for Weatherford and then for Baker Hughes in Iraq. He holds bachelor's and master's degrees in petroleum engineering from the University of Baghdad, Iraq, and a master's degree from Missouri University of Science and Technology. Al Saedi is a member of SPE.

Ralph E. Flori is an associate professor of petroleum engineering in the Geosciences and Geological and Petroleum Engineering Department at Missouri University of Science and Technology. He primarily teaches reservoir-engineering and well-testing courses. A campus leader at the Missouri University of Science and Technology, Flori has served as an assistant and associate dean of engineering, a chair and interim chair of three departments, and a leader of Project Lead the Way and other K–12 recruiting programs. He has received more than 25 different teaching awards, including the American Society of Engineering Education National Outstanding Teaching Award in 2005. Nationally recognized as an educational leader, Flori served from 2010 to 2012 as the vice president of member affairs for the American Society of Engineering Education.

C. Shah Kabir is a lecturer in petroleum engineering at the University of Houston. He teaches reserves determination at the graduate level and teaches the undergraduate Capstone class. Kabir's teaching and research interests are in reservoir, production, and drilling engineering. He has worked for 40 years in major operating and service companies, including Chevron and Schlumberger. An SPE Honorary Member, Kabir has authored or coauthored more than 140 papers. In 2018, he coauthored the second edition of the SPE book *Fluid Flow and Heat Transfer in Wellbores*.